THE IMPACT OF CHANGES IN OPERATIONAL PARAMETERS ON NITROGEN ADDITION DURING THE FORMATION OF THIN FILMS OF TiCN

Gaudencio, C.B.[1]; Oliveira, C.A.M.[1]; Grigorov, K.G.[2], Massi, M.[1]; Lima, C.R.C.[1]
[1]School of Engineering, Mackenzie Presbyterian University, São Paulo, SP, Brazil.
camilabgaudencio@gmail.com; carlos.oliveira@mackenzie.br;
marcos.massi@mackenzie.br; carlos.lima@mackenzie.br

[2]Space Research and Technology Institute, Bulgarian Academy of Sciences, Acad. G. Bonchev, Sofia, Bulgaria
kgrigoro@abv.bg

ABSTRACT

This paper presents the influence of changing operational parameters during the process of adding nitrogen to create TiCN films. These films are deposited onto steel substrates using DCMS and RFMS Magnetron Sputtering sources. The TiC and TiCN compositions are made by combining Ti and C targets with N_2 and Ar fluxes. The composition, microstructure, and thickness of the different conditions were analyzed using X-Ray Diffraction, Scanning Electron Microscopy, Raman Spectroscopy, and Profilometry. The results demonstrated that homogeneous TiC thin films were produced, with thicknesses ranging from 120 to 570 nm. Additionally, TiCN films were produced, with thicknesses varying from 120 to 140 nm. Moreover, all films exhibited a uniform distribution of elements on the surface of the substrate.

KEYWORDS: *Titanium carbide, nitrogen, titanium carbonitride, thin films, Magnetron Sputtering.*

I. INTRODUCTION

In recent decades, researchers have extensively studied thin films of titanium carbide (TiC) and titanium carbonitride (TiCN) due to their versatility and potential for various industrial applications. The superior mechanical properties of these films are considered technologically important [1]. Steel tools coated with thin layers of TiC have been adopted in manufacturing industries to enhance the efficiency and operational life of cutting tools, increasing productivity. The utilization of titanium carbide films has become prevalent in turning and milling operations involving steels and cast iron. The incorporation of a TiC layer serves to minimize the friction coefficient and improve wear resistance. [2]. These attributes have been demonstrated to enhance cutting speed by 50 to 100%, deliver 2 to 3 times greater wear resistance, reduce cutting force by 15 to 20%, and decrease heat generation during machining when compared to conventional, uncoated carbide inserts. [1].

Studies of the heat transfer generated during the cutting motion in the tool shank during machining indicates that the heat needs first to pass through the coating before flowing to the tool die. This concludes that the coating material and thickness can influence the cutting temperature distribution of the tool body [3]. Tribological investigations into TiN/Ti multilayer coatings have demonstrated reduced friction coefficients and heightened wear resistance, particularly with the deposition of 25 nm Ti layers. [2].

Daniel and colleagues conducted the deposition of coatings comprising titanium carbide/carbon using a hybrid PVD-PECVD process, which involved sputtering titanium in an atmosphere containing acetylene. Changes in energy flux affected the grain size, lattice parameter, and mean grain separation. The decrease in grain size, attributed to a higher average energy flux per unit of the coating's thickness, resulted in an increase in hardness by approximately 20-30% [4]. In the study conducted by Balázsi,

various thin films of TiC were deposited. The results indicated an increase in titanium content with the rising power of the source, manifesting a discernible impact on the microstructure of the film [5].

On the other hand, TiCN films illustrates outstanding thermal and chemical stability, elevated hardness, superior tribological behavior, heightened wear resistance, excellent thermal conductivity, and a low thermal expansion coefficient. These qualities position them as effective alternatives for cutting tools. [6, 7]. In recent years, there has been a notable advancement in the development of TiCN owing to its enhanced mechanical properties in contrast to conventional TiN and TiAlN films. The heightened resistance to abrasion in TiCN is ascribed to the elevated hardness exhibited by TiN. TiCN thin films find primary application in milling and threading operations [7, 8]. Majority of industrial cutting tools integrate some type of surface coating. Tools with coatings demonstrate superior mechanical properties, including hardness, wear resistance, and thermal stability, compared to their uncoated counterparts. The prolonged operational life of coated tools can be attributed primarily to a structure characterized by fine grains and increased surface hardness. The development of cutting tools featuring diverse coatings is vital for the efficient machining of advanced materials. Overall, the quality of any coating relies on optimized process parameters such as particle size, chemical composition, substrate temperature, voltage, current density, vacuum pressure, coating rate, substrate stress during deposition, and reactive gas pressure. [9]. The most used technique for depositing thin films of TiC and TiCN is Physical Vapor Deposition by Magnetron Sputtering. This technique involves the ejection of atoms from the surface by momentum transfer from Ti and C targets, bombarding them with energetic ion particles accelerated by plasma, and the subsequent condensation of the ejected atom onto the substrate surface [10, 11], and the energy from ion bombardment can be comparable to the magnitudes of the applied voltage [12]. As the negative substrate bias increases, ion bombardment on the substrate surface is intensified due to the increased impact energy of energetic ions in the plasma. Moreover, ion bombardment shows a delicate connection with film growth concerning the migration of adatoms and the development of metastable phases in a non-equilibrium condition. A significant impact on the surface consistently leads to a rugged surface morphology, accompanied by a higher sputtering yield attributed to residual stress [13]. The transferred energy can be determined by controlling the flux and the energy of bombarding particles (ions and neutrals). However, it is essential to note that the total energy delivered to a growing surface includes other components, such as the exothermic energy released due to compound formation, heat from the magnetron source, and plasma radiation [1]. In study of Ou, Y.X., superhard and resilient Ti-C-N coatings showcase improved water-lubricating performance in a 3.5 wt% NaCl aqueous solution, demonstrating an exceptionally low coefficient of friction at 0.03 and maintaining a stable open circuit potential of -0.05 V. The heightened surface wettability, coupled with enhanced resistance to crack initiation, propagation, and adhesion failure, plays a pivotal role in augmenting the tribocorrosion resistance properties of TiCN coatings [13].

According to Qin et al., TiCN nanocomposite coatings were produced through reactive plasma spraying, employing varying Ti/graphite ratios. The analysis revealed the presence of nano-sized TiC_xN_{1-x} ($0 \leq x \leq 1$) main phases, along with a small quantity of Ti_2O, amorphous graphite, and CN_x phases in all coatings. As the Ti/graphite ratio increases, the TiCN phase initially experiences an increase and subsequently undergoes a decrease. Furthermore, the coatings exhibit low friction coefficients and wear volumes. Overall, the deposited TiCN coatings demonstrate a combined wear mechanism involving adhesive and abrasive wear [14].

This research aims to investigate the influence of operational parameters on the nitrogen addition to TiC for the formation of TiCN thin films (nanofilms) using magnetron sputtering, employing both DCMS (Direct Current Magnetron Sputtering) and RFMS (Radio Frequency Magnetron Sputtering). The films are designed for a low friction coefficient and high wear resistance, which will be tested at the end of the study. Most of the articles found in the literature use C_2H_2, CH_4 or a mixture of gases as the carbon source [6,15,16] whereas this study used solid carbon targets and compare the carbon deposition rates.

II. EXPERIMENTAL PROCEDURE

The experimental procedure involved using AISI/SAE 4340 steel as the substrate, chosen due to its wide application in the industry. The steel samples had a diameter of 2.2 cm and a thickness of 3.0 mm. Alongside the steel, two silicon plates were positioned as substrates for X-ray diffraction and

profilometry measurements. To deposit the materials, commercial titanium (99.99%) and carbon (99.99%) targets from Process Materials Inc (Livermore, CA, USA) were applied. The targets had a diameter of 50.4 mm, and a thickness of 6.30 mm. For sputtering, a titanium target was used in the DC source, and a carbon target was used in the RF source, as illustrated in Figure 1. The thin films were deposited using a Magnetron Sputtering plasma reactor equipped with DC, RF, and HiPIMS sources. The plasma reactor was manufactured by Kurt J. Lesker Co (Pittsburg, PA, USA).

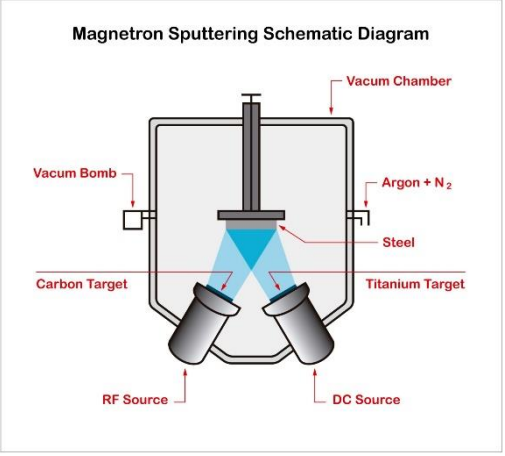

Figure 1. Diagram of the Magnetron Sputtering setup that was used in the study.

The researchers sanded and polished the samples (with abrasives sheets with grit sizes of 200, 400, 600 and 1200) before immersing them in acetone and subjecting them to ultrasonic cleaning for 20 minutes. This process was performed to eliminate surface impurities. After completing the cleaning procedure, the samples were placed in the reactor.

The deposition was carried out under vacuum in an argon atmosphere at room temperatures (T_{room}) and at 200, 300 and 400 °C. The target-substrate distance was set at 21 cm, without rotation. The base pressure was $5.0x10^{-6}$ torr, and the working pressure was maintained at $5.0x10^{-3}$ torr for all the samples. The initial stage of TiC deposition involved parameter and equipment adjustments before the introducing nitrogen.

In the second stage, Ti and C were deposited in a vacuum environment with Ar and N_2 for the formation of TiCN, at temperatures of 200 and 300 °C. The source power and Ar flow were varied, and N_2 was introduced. The third stage included depositing Ti and C in a vacuum environment with Ar and N_2 to form TiCN at a temperature of 200 °C, following the same conditions as the second stage but with substrate bias. Table 1 illustrates the parameter conditions for the stages.

Table 1: Parameters for the first, second, and third stages of the deposition of TiC and TiCN thin films in different environments.

Stages	Samples	Temperature (°C)	Power RF (W) C	Power DC (W) Ti	Time (min)	Ar flow (sccm)	N_2 flow (sccm)	Bias (v)
First	C1	Room	180	80	90	35	-	-
	C2	200	200					
	C3	300						
	C4	400						
Second	N200	200	220	90	120	30	5	-
	N300	300						
Third	N200 -60	200						-60
	N200 -30							-30

X-ray diffraction analysis was conducted using Rigaku Miniflex equipment (Austin, TX, USA), with a Cu target and radiation source (λ = 1.540598 Å). The diffraction angle (2θ) ranged from 20 to 70°, with a scanning speed of 0.06° s^{-1}, to confirm the presence of TiC and TiCN. Furthermore, Raman spectroscopy using Witec Alpha 300 (Ulm, Germany) was performed to verify this information. The samples were excited using a 532 nm laser with a power of 2.5 mW.
Thickness analysis was performed using a Taylor Hobson profilometer, Form Talysurf Intra (Leicester, England). The microstructure and morphology of the films were examined using the JEOL JSM-6510 scanning electron microscopy (SEM) instrument (Tokyo, Japan), equipped with energy-dispersive X-ray spectroscopy (EDS).

III. RESULTS AND DISCUSSION

3.1. X-ray Diffraction

In the first step, X-ray diffraction analysis performed on a silicon substrate revealed the formation of thin TiC films at three different diffraction angles in all tested samples, as shown in Figure 2 (a). The peak at 33.3° is silicon from the substrate, appearing with higher intensity in sample C4. It is also present in C1 and C2 as a TiC space group but disappears in C3. The graph shows that in C1, it is shifted to a higher 2θ, indicating that the cubic space group FM3M experiences a lack of specific carbon atoms for this outer plane (111). Upon leaving the vacuum chamber, it easily oxidizes, forming titanium sub-oxide (TiO). All other samples have the correct position, but only C4 shows less Full Width at Half Maximum (FWHM), meaning a slimmer peak width in the intensity distribution, indicating a better-oriented crystalline structure, such as the absence of defects.

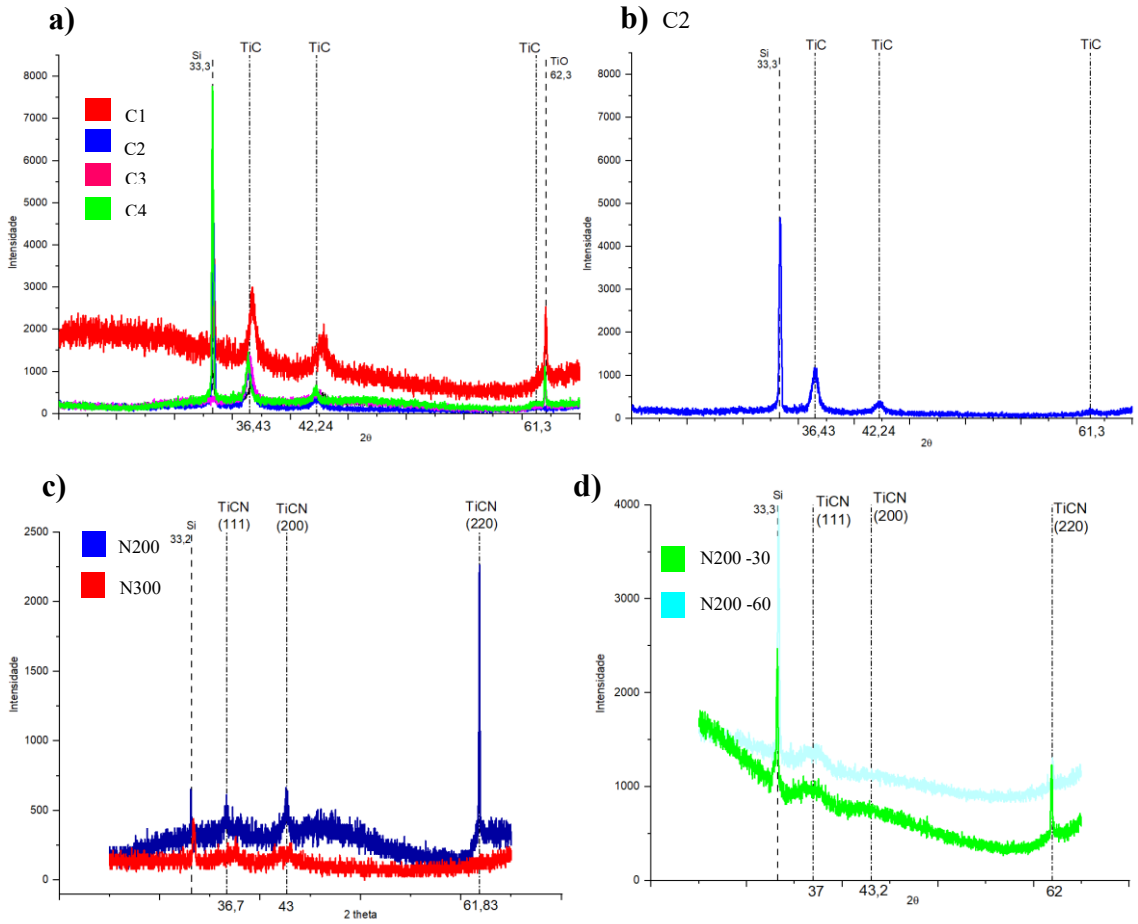

Figure 2: X-ray diffractograms: (a) of the samples deposited with TiC thin films at room temperature, 200, 300 and 400 °C; (b) C2 at 200 °C; (c) of TiCN at 200 °C and 300 °C; (d) of TiCN at 200 °C with -30 and -60 v bias.

Regarding the general spectra, the peaks at 41.89° correspond to the TiC (200) plane, and the peak at 61.2° is from the TiC (220) plane. As the z-axis is perpendicular to the substrate, this reflection is greatly

reduced. At 61.9°, the TiO (220) plane is evident, which has "z" axes parallel to the substrate. Therefore, even in smaller quantities, this reflection is strong. This does not apply to sample C2, which is not oxidized. Hence, sample C2, Figure 2 (b), represents the best temperature choice, as higher temperatures cause strong H_2O emission from the substrate support and the chamber.

In the second stage, a TiCN thin film formed at three different diffraction angles in the tested samples, as depicted in Figure 2(c). The peak at ~37° corresponds to TiCN in the (111) plane, with higher intensity in the N200 sample, appearing with lower intensity in N300 and shifted 2θ higher in N300 compared to N200. This change might arise from substituting smaller-sized nitrogen atoms for carbon atoms within the solid solution [17].
The peak at ~36° represents the (111) plane of either TiC or cubic TiN, as both have very similar peak values. The peak at ~44° is the peak of the (200) plane of TiCN. It can be observed that at both temperatures, the peaks have low intensity, indicating lower crystallinity of the film structure [18]. At ~61°, the (220) plane peak of TiCN is observed in N200, which does not occur in N300. The widening of the peak at N300 may be linked to heightened stress or an enlargement in crystalline size [17].

In the third stage, nitrogen was added, and the bias was varied (-30 V and -60 V). Diffractometry analysis showed the formation of a TiCN thin film at two different diffraction angles in the tested samples, as shown in Figure 2(d). The peak at ~37° indicates TiCN in the (111) plane with similar intensities in both samples. However, the samples exhibited broader peaks, which may indicate lower crystallinity. The peak at ~44° of the (200) plane of TiCN was not observed in both samples. At ~61°, the peak of the (220) plane of TiCN was observed in N200 -30 and N200 -60, with greater intensity in the N200 -30 sample and a more elongated peak, indicating better crystallinity compared to N200 -60 [19]. The possible explanation is that ions with higher energy penetrate the film, leading to the formation of defects and the generation of compressive stress. This stress, in turn, induces lattice distortion and results in a damaged film [20].

3.2. SEM and EDS

The EDS images revealed thin films with good homogeneity of the added elements in all the samples. There was no difference in homogeneity due to the addition of nitrogen. In the first stage samples, the elements Ti, C, and O were found in the film. Titanium and carbon were deposited, while oxygen was present due to their release from the sample holder, the chamber, and the substrate.

In the second and third stage samples, even with the addition of nitrogen, the homogeneity remained consistent across all samples. Figure 3 displays EDS images of the N200 -60 sample, where the film surface appears to remain consistently smooth.

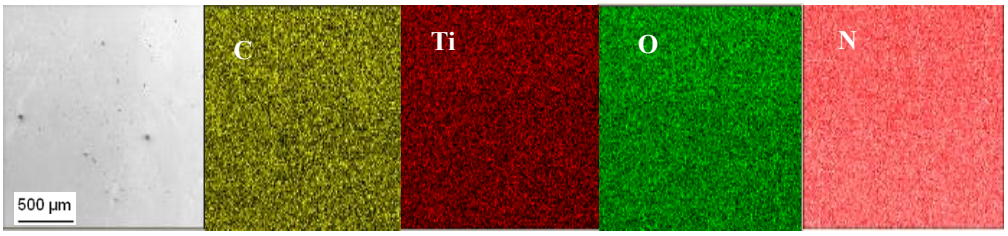

Figure 3: EDS images of the Ti, C, N and O elements present in sample N200 -60.

3.3. Profilometry

Profilometry analysis was conducted to measure the thickness of the samples. The measured thickness of sample C1 was 195 nm, while sample C2 at 200 °C had a thickness of 570 nm. Sample C3 at 300 °C exhibited a thickness of 120 nm, which is lower than the measurement at lower temperatures. Sample C4 at 400 °C had a very low thickness (immeasurable) and was not of interest for the study's focus. The thicknesses are detailed in Table 2, where they are compared with the deposition temperature of the samples.

Table 2: Thickness measurements as a function of deposition temperature for the TiC, "C" samples from the first stage, the N200 and N300 samples from the second stage and the N200 -30 and N200 -60 samples from the third stage.

Sample	Temperature (°C)	Thickness (nm)
C1	T_{room}	195
C2	200	570
C3	300	120
C4	400	-
N200	200	140
N300	300	125
N200 -30	200	130
N200 -60	200	120

In the second stage, measurements were taken for the N200 samples at 200 °C and the N300 samples at 300 °C, both with nitrogen. A higher thickness was recorded at 200 °C, approximately 12% higher than at 300 °C, indicating that the thickness decreases with increasing temperature. In the third stage, measurements were conducted for the N200 -30 and N200 -60 samples. A thickness of 130 nm was obtained for the sample at 200 °C and -30 V, 8% greater than at -60 V, indicating that the thickness decreased with the increase in negative bias.

This tendency of reduction in TiCN coating thickness observed in the N200 samples has been reported in previous works. The probable cause for this is the resputtering effect resulting from ion bombardment or surface growth induced by incident ions, stemming from the negative bias applied to the substrate [21].

3.4. Raman Spectroscopy

Stoichiometric TiC lacks active Raman vibrational modes. Nevertheless, bands arising from nitrogen and carbon vacancies, along with other defects, become apparent in TiCx. Vacancies have the potential to disturb the symmetry of optical isomers in proximity and lead to broader first-order Raman scattering [14, 21]. Crystallized samples near the stoichiometric composition demonstrate only faint second-order Raman scattering in the experimental spectra. The elevated relative percentage of lattice defects in such coatings enables the identification of defect-induced Raman spectra [22]. The intensity, frequency, and width of Raman features are significantly influenced by the chemical composition, defects, short-range order, crystalline structure, and internal stresses present in the material [23].

Figure 4(a) shows the Raman spectrum of the C2 sample. Bands related to TiC were observed between 200 and 400 cm^{-1}, where pure metallic titanium is present, exhibiting a broad low-frequency band or scattering in the transversal (TA) and longitudinal (LA) acoustic range. This is attributed to the collective vibrations of the titanium atoms in the crystalline structure. Between 600 and 700 cm^{-1}, where the TiC (Ti-C) band emerges, associated with the vibrations of the bonds between the titanium and carbon atoms in the TiC structure, transversal (TO) and longitudinal (LO) optical scattering. Due to the very thin thickness, unidentified bands in the spectrum were generated, which were discarded as cosmic rays (noise) [21, 23]. To enhance the comprehension of the structure of TiC films, Raman spectra in the 100 - 800 cm^{-1} range were fitted with four Gaussian bands. These Raman shifts align with previously published results [22].

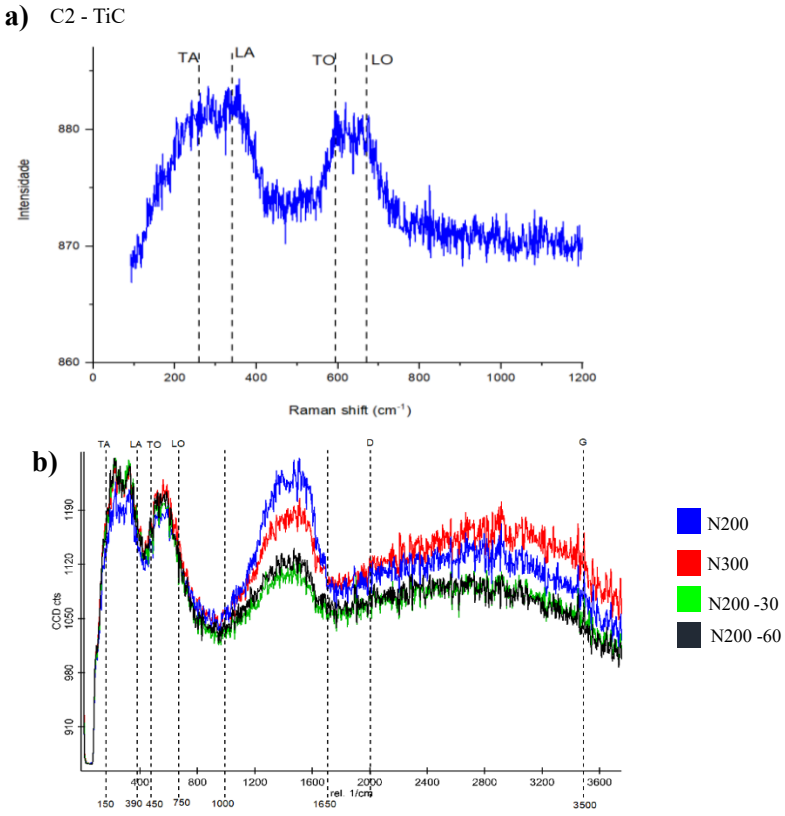

Figure 4: (a) Raman spectrum of sample C2, with transversal (TA) and longitudinal (LA) acoustic scattering peaks and transversal (TO) and longitudinal (LO) optical scattering peaks. (b): Raman spectra of samples N200, N300, N200 -30 and N200 -60, with the Ti, C and N peaks.

In recent studies, Raman findings have been documented regarding TiC1-xNx coatings, revealing specific alterations in the frequency of various Raman features with changes in the C:N ratio within the coatings [23]. Figure 4(b) illustrates the Raman spectra of the N200, N300, N200 -30, and N200 -60 samples. The peaks at 150 and 750 cm^{-1} denote pure titanium, while those between 1000 and 1650 cm^{-1} are associated with carbon and nitrogen, signifying the formation of TiCN. The wide band between 2000 and 3500 cm^{-1} corresponds to amorphous carbon, a result of the overlapping spectra of the D and G modes of graphite. Although the intensity of these bands might decrease with rising temperature, suggesting a potential enhancement in crystal quality [21], in this case, the band intensities remained unaltered.

Concerning the N200 samples with -30 V and -60 V bias, no shifts in band positions were observed with increasing bias. According to AitDjafer et al., alterations in substrate bias produce continuous shifts in Raman band positions, particularly notable in the acoustic phonon range, where bands shift to higher frequencies with an augmented substrate bias. While the variation in substrate bias was more significant in that study compared to this one, the entire set of bands in this study demonstrated changes in position and intensity with increasing substrate bias, indicating an enhancement in crystal quality and a probable increase in carbon content. As carbon content rises, acoustic phonons shift to higher frequencies due to alterations in the lattice constant [22, 23].

IV. CONCLUSIONS

Based on the results obtained, the following conclusions can be drawn:

Thin films of TiCN were successfully deposited using Magnetron Sputtering. This was achieved by employing two solid targets, one containing Ti and the other containing C, and utilizing a mixture of argon and nitrogen as the deposition gas.

It was observed that the optimal temperature for TiCN deposition is 200 °C, with a deposition time of 140 minutes. The gas flow rates of 5 sccm of N_2 and 30 sccm of Ar were found to be the most suitable for the deposition process.

X-Ray Diffractograms confirmed the presence of (111), (200), and (220) planes in samples N200 and N300, and (111) and (220) planes in samples N200 -30 and N200 -60. It was observed the successful formation of the crystalline structure, however, it is important to highlight that the presence of amorphous carbon was also identified, as evidenced by the Raman spectrum. This coexistence of crystalline and amorphous structures adds a layer of complexity to the understanding of the composition and properties of the studied films.

All samples analyzed by profilometer showed very thin films, with thicknesses ranging from 120 to 195 nm. Sample C2 had a thickness of 570 nm, as it did not oxidize due to the strong water emission from the support and chamber caused by the increase in temperature, resulting in the formation of TiO.

Raman spectra exhibited bands related to both TiC and TiCN, with high intensities and elongated bands, indicating good crystal quality. Nitrogen-containing samples showed the presence of amorphous carbon, suggesting that nitrogen might have replaced carbon in the crystal lattice, what is not convenient, as a higher nitrogen content promotes film delamination, while carbon provides better adhesion.

ACKNOWLEDGEMENTS

This study was partially financed by the Coordenação de Aperfeiçoamento de Pessoal de Nível Superior – Brasil (CAPES) – Finance Code 001

REFERENCES

[1]. Larhlimi, H., Ghailane, A., Makha, M. & Alami, J., (2022) “Magnetron sputtered titanium carbide-based coatings: A review of science and technology”, *Vacuum*, Vol. 197, pp. 110853 (https://doi.org/10.1016/j.vacuum.2021.110853).

[2]. Badiger, P.V., Desai, V., Joladarashi, S. & Gourkar, H. (2019) “Tribological behavior of monolayer and multilayer Ti-based thin solid films deposited on alloy steel”, *Mater. Res. Express*, Vol. 6, No. 2, pp. 026419 (DOI 10.1088/2053-1591/aaef6d).

[3]. Zhang J., Zhang G. & Fan G. (2022) “Effects of tool coating materials and coating thickness on cutting temperature distribution with coated tools”, Int. J. Appl. Ceram. Tec., Vol. 19, No. 4, pp. 2276-2284, (https://doi.org/10.1111/ijac.14038).

[4]. Daniel, J., Souček, P., Zábranský, L., Buršíková, V., Stupavská, M. & Vašina, P., (2017) “On the effect of the substrate to target position on the properties of titanium carbide/carbon coatings”, Surf. Coat. Techol. Vol. 328, pp. 462-468 (https://doi.org/10.1016/j.surfcoat.2017.06.076).

[5]. Balázsi, K. (2019) “Magnetron sputtered TiC/a:C nanocomposite thin films: Deposition parameters vs. properties”, *Vacuum*, Vol. 164, pp. 121-125. (https://doi.org/10.1016/j.vacuum.2019.03.012).

[6]. Shafyei, H. & Ashiri, R. (2019) “Electron beam assisted physical vapor deposition of very hard TiCN coating with nanoscale characters”, *Ceram. Int.*, Vol. 45, No. 12, pp. 14821-14828, (https://doi.org/10.1016/j.ceramint.2019.04.213).

[7]. Akinribide, O. J., Obadele, B. A., Akinwamide, S. O., Bilal, H., Ajibola, O. O., Ayeleru, O. O., Ringer, S. P. & Olubambi, P. A. (2019) “Sintering of binderless TiN and TiCN-based cermet for toughness applications: Processing techniques and mechanical properties: A review”, *Ceramics International*, Vol. 45, pp. 21077-21090, (https://doi.org/10.1016/j.ceramint.2019.07.191).

[8]. Das S., Guha S., Das P.P. & Ghadai R.K. (2020) “Analysis of morphological, microstructural, electrochemical, and nanomechanical characteristics of TiCN coatings prepared under N_2 gas flow rate by chemical vapor deposition (CVD) process at higher temperature”, *Ceram. Int*., Vol. 46, No. 8, pp. 10292-10298 (https://doi.org/10.1016/j.ceramint.2020.01.023).

[9]. Bakalova, T., Svobodová, L., Petkov, N., Bahchedzhiev, H., Švec, M. Kejzlar, P., Šutta, P., & Daďourek, K. (2023) “The effect of the process gas mixture ratio on the structure and composition of TiC and TiCN

thin layers prepared by cathodic arc deposition on tool steel", *Journal of Manufacturing Processes*, Vol. 93, pp. 90-100 (https://doi.org/10.1016/j.jmapro.2023.02.067).

[10]. Kumar T.S., Jebaraj, A.V., Tamiloli, N. & Sivakumar, K. (2019) "Metallurgical and mechanical characterization of TiCN/TiAlN and TiAlN/TiCN bilayer nitride coatings", Surf. Interf., Vol. 15, pp. 256-264 (https://doi.org/10.1016/j.surfin.2019.03.001).

[11]. Abegunde O.O., Esther A., Oladijo O.P. & Majumdar J.D. (2019) "Surface integrity of TiC thin film produced by RF magnetron sputtering", Procedia Manuf., Vol. 35, No. 1, pp. 950-955 (https://doi.org/10.1016/j.promfg.2019.06.040).

[12]. Suresh, U., Parasuraman K., Ramaseshan R. & Dhanalakshmi S. (2021) "Structural, nanomechanical, and electrochemical properties of TiC and TiN films prepared by pulsed DC magnetron sputtering technique", Mater. Today-Proc., Vol. 47, No. 23, pp. 1091-1098 (DOI: 10.1016/j.matpr.2021.07.124).

[13]. Gudmundsson, J. T., Anders, A. & von Keudell, A. (2022) "Foundations of physical vapor deposition with plasma assistance", Plasma Sources Science and Technology, Vol. 31, No. 8, pp. 083001 (DOI: 10.1088/1361-6595/ac7f53).

[14]. Kenzhegulov A., Mamaeva, A., Panichkin, A., Alibekov, Z., Kshibekova, B., Bakhytuly, N. & Wieleba, W. (2022) "Comparative Study of Tribological and Corrosion Characteristics of TiCN, TiCrCN, and TiZrCN Coatings", Coatings, Vol. 12, No. 5, pp. 1-15 (https://doi.org/10.3390/coatings12050564).

[15]. Ou, Y. X., Wang, H. Q., Hua, Q. S., Liao, B. & Ouyang, X. P. (2022) "Tribocorrosion behaviors of superhard yet tough Ti-C-N ceramic coatings", Surface and Coatings Technology, Vol. 439, pp. 128448 (https:// doi.org/10.1016/j.surfcoat.2022.128448).

[16]. Saoula N., Madaoui, N., Tadjine, R., Erasmus, R. M., Shrivastava, S. & Comins, J. D. (2016) "Influence of substrate bias on the structure and properties of TiCN films deposited by radio-frequency magnetron sputtering", Thin Solid Films, Vol. 616, pp. 521-529 (https://doi.org/10.1016/j.tsf.2016.08.047).

[17]. Qin, Y., He, Z, Zhao, H., Song, J., Lu, J., Ma, Z. & He, J. (2022) "Study on the microstructure and mechanical properties of reactive plasma sprayed TiCxN1−x composite coatings with different Ti/graphite powders", Diamond & Related Materials, Vol. 126, pp. 109028 (https://doi.org/10.1016/j.diamond.2022.109028).

[18]. Chen R., Tu, J., Liu, D., Mai, Y. & Gu, C. (2011) "Microstructure, mechanical and tribological properties of TiCN nanocomposite films deposited by DC magnetron sputtering", Surf. Coat. Tech., Vol. 205, No. 21-22, pp. 5228-5234 (https://doi.org/10.1016/j.surfcoat.2011.05.034).

[19]. Aihaiti, L., Tuokedaerhan K., Sadeh, B., Zhang, M., Shen, X. & Mijiti, A. (2021) "Effect of annealing temperature on microstructure and resistivity of TiC thin films", Coatings, Vol. 11, No. 4, pp. 457 (https://doi.org/10.3390/coatings11040457).

[20]. Mamaeva A., Kenzhegulov A., Panichkin, A., Alibekov, Z. & Wieleba, W. (2022) "Effect of Magnetron Sputtering Deposition Conditions on the Mechanical and Tribological Properties of Wear-Resistant Titanium Carbonitride Coatings", Coatings, Vol.12, No. 2, pp. 193 (https://doi.org/10.3390/coatings12020193).

[21]. Qi, Q., Zhang, W.Z., Shi, L.Q., Zhang, W.Y., Zhang, W. & Zhang, B. (2012) "Preparation of single-crystal TiC (111) by radio frequency magnetron sputtering at low temperature", Thin Solid Films, Vol. 520, No. 23, pp. 6882-6887 (https://doi.org/10.1016/j.tsf.2012.07.040).

[22]. Ait Djafer, A.Z., Saoula N., Madaoui N. & Zerizer A. (2014) "Deposition and characterization of titanium carbide thin films by magnetron sputtering using Ti and TiC targets", Appl. Surf. Sci., Vol. 312, pp. 57-62 (https://doi.org/10.1016/j.apsusc.2014.05.084).

[23]. Dreiling, I., Stiens, D. & Chassé, T. (2010) "Raman spectroscopy investigations of TiBxCyNz coatings deposited by low pressure chemical vapor deposition", Surf. Coat. Tech., Vol. 205, No. 5, pp. 1339-1344 (https://doi.org/10.1016/j.surfcoat.2010.09.022).

[24]. Dreiling I., Haug, A., Holzschuh, H. & Chassé, T. (2009) "Raman spectroscopy as a tool to study cubic Ti-C-N CVD coatings", Surf. Coat. Tech., Vol. 204, No. 6-7, pp. 1008-1012 (https://doi.org/10.1016/j.surfcoat.2009.05.029).